ChemComm

COMMUNICATION

View Article Online
View Journal | View Issue

Cite this: *Chem. Commun.*, 2017, 53, 12406

Received 23rd October 2017,
Accepted 30th October 2017

DOI: 10.1039/c7cc08162f

rsc.li/chemcomm

Dual-target cancer theranostic for glutathione *S*-transferase and hypoxia-inducible factor-1α inhibition†

Zan Li,[a] Jie Ding,[b] Chunxia Chen,[a] Jiayin Chang,[a] Binghuan Huang,[a] Zhirong Geng *[a] and Zhilin Wang *[a]

We developed a dual-target theranostic F_{671}, which could exhibit synergetic anticancer effects for inhibiting the activities of glutathione *S*-transferase and the accumulation of hypoxia inducible factor-1α. F_{671} undergoes self-immolative cleavage when exposed to GSTP1-1 in live cancer cells, facilitating the visualization of molecule release and distribution, as well as confirming the autophagy-induced apoptosis.

Cancer is one of the most intricate and refractory diseases with increasing morbidity in the world, and chemotherapy remains the primary option for cancer therapy. Exposure to anticancer agents may lead to drug resistance, a key element in the failure of chemotherapy.[1] Therefore, it is critical to develop effective strategies to overcome drug resistance for cancer treatment.[2]

Previous studies revealed that glutathione *S*-transferases (GSTs) have been implicated in the development of carcinogenesis and drug resistance, concluding that GSTs can be destined as protein markers for cancer.[3] Among the different GST isoenzymes, GSTP1-1 has received the most attention because of its high levels in tumors.[4] Hypoxia inducible factor-1α (HIF-1α), which upregulates the expression of genes associated with tumor initiation, malignant progression, metastasis, and resistance to radiotherapy and chemotherapy, is overexpressed in several human cancers.[5,6] Targeting HIF-1α has been proven to significantly slow tumor growth in xenograft models and render hypoxic cells more susceptible to conventional therapies.[7] Given the significant roles of GST and HIF-1α in the drug resistance of human cancers, a growing number of therapeutic agents that target GST and HIF-1α have gained considerable traction and attention in the medical and scientific communities.[8]

Theranostics, combining diagnosis with targeted therapy in one molecular system, have received considerable attention in recent years.[9a–c] However, the problem of drug resistance when using a mono-target molecular system is still unresolved.[9d] Synchronous administration of multiple drugs is an attractive way to maximize therapeutic efficacy and minimize the occurrence of multidrug resistance compared to mono-drug treatment. Right now the design and synthesis of dual-target cancer theranostics for enhanced synergetic anticancer efficacy is still challenging.

The synthesized compounds, F_{671} and F_{335}, were characterized by ^{1}H NMR, ^{13}C NMR and ESI-MS. 7-Nitro-2,1,3-benzoxadiazol (NBD) was introduced into F_{671} due to its GSTP1-1 targeting and inhibiting abilities. Furthermore, the high fluorescence of F_{508} (Φ = 0.192) could be quenched by NBD (Fig. S1, ESI†).[10,11] It is anticipated that upon initiation of F_{671} (Φ = 0.025) by GSTP1-1, subsequent cleavage of the linker occurs to afford F_{508}, and the HIF-1α level could be decreased simultaneously. In the meantime, the enhanced fluorescence allows for GSTP1-1-overexpressed cancer cells to be imaged and identified (Scheme 1).

The apparent dissociation constant of F_{671} and GSTP1-1 in the presence of GSH is 75.79 μM (Fig. S2, ESI†).[10a] This value is close to the order of magnitude for the IC_{50} value found for cancer cell lines (Table S1, ESI†). The affinity of F_{671} toward GSTP1-1 distinctly decreased (K_d 877.26 μM) in the absence of

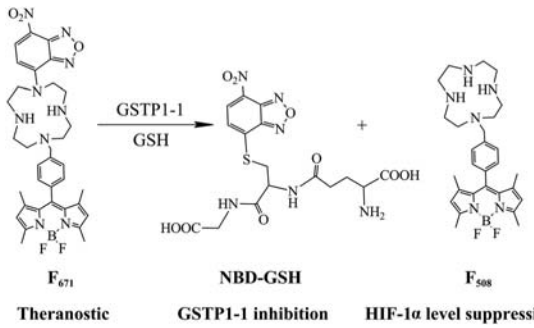

Scheme 1 Proposed mechanism of the reaction of GSTP1-1 in the presence of GSH.

[a] *State key Laboratory of Coordination Chemistry, School of Chemistry and Chemical Engineering, Collaborative Innovation Center of Advanced Microstructures, Nanjing University, Nanjing 210093, P. R. China. E-mail: gengzr@nju.edu.cn, wangzl@nju.edu.cn*

[b] *Department of General Surgery, Nanjing Drum Tower Hospital, The Affiliated Hospital of Nanjing University Medical School, Nanjing 210008, P. R. China*

† Electronic supplementary information (ESI) available. See DOI: 10.1039/c7cc08162f

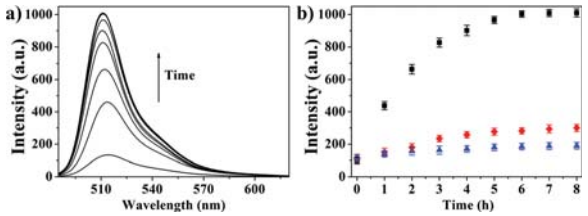

Fig. 1 Spectroscopic properties of F_{671} (10 μM) in Tris–HCl (0.02 M) solution (DMSO/Tris–HCl = 1 : 9 v/v, pH 7.4) at 37 °C. (a) Time-dependent fluorescence spectra of F_{671} to GSTP1-1 (5 U) in the presence of GSH (1 mM). (b) Time-dependent fluorescence intensity of F_{671}. (■), in the presence of GSTP1-1 (5 U) and GSH (1 mM). (◆), in the presence of GSTP1-1 (5 U), GSH (1 mM) and TER 199 (200 μM). (▲), in the presence of GSH (1 mM). The excitation wavelength was 480 nm. The error bars represent ±S.D. (n = 3).

GSH, which demonstrated that GSH is vital in the GST inhibition of F_{671}. The relative fluorescence intensity of F_{671} is stable in the pH range 7.0–10.0 (Fig. S3, ESI†), which clearly demonstrated that F_{671} is stable under physiological conditions. After incubating F_{671} with GSTP1-1 and GSH, the fluorescence exhibited a steady enhancement (Fig. 1a). However, upon adding the potent GSTP1-1 inhibitor TER 199 into the former system, the fluorescence did not change significantly.[4] Similarly, the interaction between F_{671} and GSH (without GSTP1-1) yielded negligible fluorescence changes (Fig. 1b). The results indicated that GSTP1-1 initiated the decloaking of F_{671} and revealed free F_{508} in the presence of GSH. The proposed mechanism is shown in Scheme S2 (ESI†).[10b] As NBD-GSH (Φ = 0.002) had low quantum yields, the fluorescence interference of NBD-GSH could be neglected in the fluorescence spectra and confocal imaging spectra (Fig. S4, ESI†).

Moreover, the ESI-MS spectra of the enzymatic reaction solution were examined. The m/z signal at 509.34 ($[M + H]^+$) represents the existence of compound F_{508} (calculated value is 509.34) and the m/z signal at 469.06 ($[M - H]^-$) represents NBD-GSH (calculated value is 469.08) (Fig. S5 and S6, Scheme S2, ESI†), further confirming the formation of F_{508} and NBD-GSH. The *in vitro* anticancer activity of F_{671} and other compounds was tested against several human cancer cell lines (HepG-2, HeLa, MCF-7, A549, and A549cisR) and the human hepatic cell line LO2 (Table S1, ESI†). F_{671} exhibited approximately 1.5-fold higher cytotoxicity against HepG-2 cells than against LO2 cells. Intriguingly, the cytotoxicity toward A549cisR was slightly higher (1.3-fold) than toward A549, which indicated that F_{671} is more efficient when treating a drug resistant cancer cell line.

GSTP1-1 is overexpressed in many cancer cell lines, where the estimated concentrations of GSTP1-1 may reach up to 50 μM.[10a] So we employed F_{671} for imaging GSTP1-1 in HepG-2 cells (Fig. 2a). The green fluorescence from the cytoplasm showed an obvious 8-fold enhancement after 6 h (Fig. 2a and c1), indicating that F_{671} was consumed by GSTP1-1 in the cytoplasm. This is consistent with evidence that the cytosolic GSTP1-1 accounts for the predominant part of the total GST protein.[12] Conversely, the fluorescence enhancement was remarkably reduced in the presence of TER 199 (Fig. 2c1). In the LO2 cells, the green fluorescence changes of F_{671} were barely recognizable from 0.5 h to 6 h (Fig. 2b and c2). The fluorescence images of F_{508} and DND-99 can be merged well in the

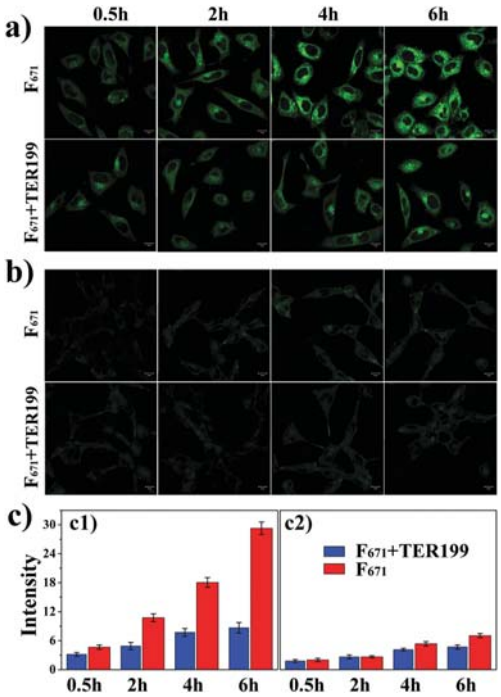

Fig. 2 Time-dependent GSTP1-1 imaging in HepG-2 cells and LO2 cells. Cells were cultured with F_{671} (1 μM) for 20 min. Confocal fluorescence images were obtained at different time points. (a) Confocal imaging after incubation of the HepG-2 cells with F_{671} (top) and TER 199 (200 μM) + F_{671} (bottom). (b) Confocal imaging after incubation of the LO2 cells with F_{671} (top) and TER 199 (200 μM) + F_{671} (bottom). (c) Quantitative analysis of the fluorescence changes of F_{671} in the absence or presence of TER 199 in panels (c1) and (c2).

colocalization experiments (Fig. S7, ESI†). The Pearson Coefficient is 0.85, which confirmed that F_{508} can specifically target the lysosomes. Above all, the experimental results demonstrated that F_{671} can be applied for the fluorescence imaging of GSTP1-1 in cancer cells and for fluorescently distinguishing cancer cells from normal cells.

The intracellular fluorescence distribution altered dramatically while incubating with F_{671} (Fig. 3). At 12 h, the green fluorescence was distributed in the cytoplasm, while at 18 h, the fluorescence was concentrated mainly in the lysosomes. The fluorescence was transformed into the green punctate dots after 24 h. Moreover, cell apoptosis was evaluated by quantitatively measuring cellular propidium iodide (PI) uptake using flow cytometry analysis. Only 2.1% of the HepG-2 cells exhibited positive PI uptake after 0.5 h (Fig. S8, ESI†), which indicated that a short time of incubation with F_{671} did not induce cell apoptosis. The percentage of PI positive cells was 99.4% at 24 h, which indicated that F_{671} caused apoptosis after a long incubation time. The co-staining and PI staining images in Fig. S9 (ESI†) indicate that F_{508} could also induce lysosome morphology variation and cell apoptosis. The integrity of the lysosome membrane in HepG-2 cells was evaluated by the activity of released β-*N*-acetylglucosaminidase (NAG). Compared with the control group, the activity of the released NAG was remarkably enhanced after treating with F_{671} and F_{508} (Fig. S10, ESI†). It is concluded that the lysosome membrane was disrupted by F_{671} and F_{508}.

To further verify the formation of F_{508} in living cancer cells, the lysosomes of the HepG-2 cells after incubation with F_{671}

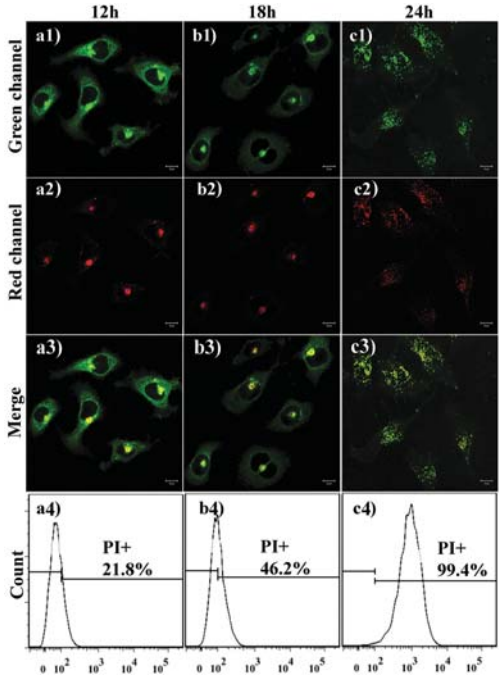

Fig. 3 Lysosome morphology variation in HepG-2 cells after different incubation times (12 h, 18 h and 24 h) with F_{671} (1 μM) treatment. (a1, b1 and c1) The green fluorescence distribution. (a2, b2 and c2) Lyso-Tracker DND-99 staining reveals the morphological alterations of the lysosomes. (a3, b3 and c3) The merged images of green fluorescence and red fluorescence. (a4, b4 and c4) Flow cytometry analyses of the propidium iodide positive cells.

were isolated. As shown in Fig. S11 (ESI†), the *m/z* signal at 509.32 ($[M + H]^+$) represents the existence of F_{508}, demonstrating the generation of F_{508} in the lysosomes of HepG-2 cells. The results supported the proposed reaction raised formerly and further confirmed the exact formation of F_{508} in living cells, as well as the distinct fluorescence response of GSTP1-1.

Previous studies revealed that nitrogen-containing molecules and metal complexes can induce autophagy in cancer cells.[13] We further investigated whether F_{671} could induce autophagy in HepG-2 cells by transmission electron microscopy (TEM).[14] Most of the cisplatin- and F_{671}-treated cells were found to display morphological characteristics of autophagy compared with the control group (Fig. S12, ESI†). Western blot analysis showed that the ratio of LC3-II/LC3-I is markedly enhanced after F_{671} treatment (Fig. S13a, ESI†).[15] Collectively, F_{671} could induce autophagic apoptosis of cancer cells and could be utilized to trace the autophagic apoptosis process with bright green fluorescence.

Our laboratory has exploited manganese complexes as neuroprotection agents based on the regulation of HIF-1α levels.[16] The effect of F_{671} on HIF-1α accumulation in HepG-2 cells was studied by western blot analysis.[17] As illustrated in Fig. 4, F_{671} suppressed HIF-1α accumulation in a dose-dependent manner. Reverse transcription-PCR analysis showed that F_{671} exerted no effect on the mRNA level of HIF-1α, indicating that the decreased concentration of HIF-1α was regulated at the protein level. As indicated in Fig. S14 (ESI†), accumulation of HIF-1α was also suppressed by F_{508} in an analogous manner to that of F_{671}, which confirmed that the inhibition of HIF-1α by F_{671} is actually

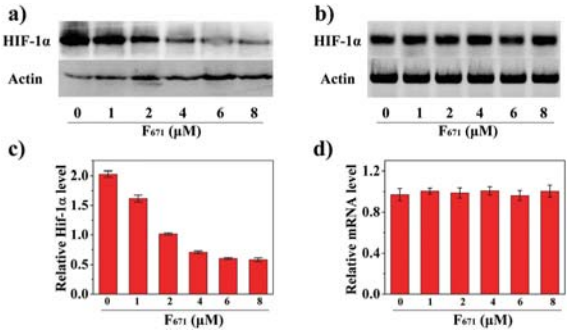

Fig. 4 Effects of F_{671} treatment on protein and mRNA levels of HIF-1α in HepG-2 cells under hypoxia (1% O_2). HepG-2 cells were incubated with various concentrations of F_{671} for 24 h. (a) Western blot analysis of HIF-1 α accumulation in whole cell extracts. β-Actin was used as a loading control. (b) RT-PCR analysis of HIF-1α gene expression. β-Actin was used as a loading control. (c) Quantification of HIF-1α protein expression levels by densitometry relative to β-actin. (d) Quantification of HIF-1α gene expression levels by densitometry relative to β-actin. The error bars represent ±S.D. (n = 3).

executed through F_{508}. Therefore, F_{508} is the key element in targeting HIF-1α.

The fluorescence intensity of dihydroethidium (DHE) in HepG-2 cells is independent of concentration and time (Fig. S15 and S16, ESI†), indicating that the generation of excess ROS does not occur in the presence of F_{508} and F_{671}. This in turn prevents the ROS-mediated inhibition of the prolyl hydroxylase domain (PHD), and consequently reduces HIF-1α protein levels under hypoxic conditions.[18] The mode of action of F_{671} can also be regarded as a restoration of PHD activity.[19] As shown in Fig. S13b (ESI†), a down-regulation of Bcl-2[20] expression was observed after treating HepG-2 cells with various concentrations of F_{671}. The active-caspase-3 (17 kDa)[21] level was enhanced with the increasing concentrations of F_{671} (Fig. S13c, ESI†). Thus, F_{671} acts as a potent inhibitor to suppress the Bcl-2 levels, while promoting the induction of apoptosis in HepG-2 cells.

The *in vivo* therapeutic efficacy of F_{671} was evaluated using tumor-bearing BALB/c mice. There was no statistically significant difference in the weight changes among the groups over 16 days (Fig. 5b). However, the tumor volume of the control group increased rapidly compared with other groups (Fig. 5a). The mice administrated with a high-dose of F_{671} showed an obvious suppression of the tumor compared to other doses (Fig. 5c), indicating effective antitumor therapy *in vivo*. In addition, there was no fluorescence signal from other organs of the F_{671}-treated group, while only the tumor was fluorescent in *ex vivo* fluorescence imaging (Fig. 5d and Fig. S17, ESI†). This enhanced fluorescence signal in the solid tumor sample indicated the tumor-specific accumulation of F_{671}, which is consistent with the *in vitro* fluorescence results in Fig. 2.

In summary, we report a novel synergetic anticancer theranostic, F_{671}, which undergoes self-immolative cleavage when exposed to GSTP1-1 in live cancer cells. Thus the imaging and distinguishing of GSTP1-1-overexpressed cancerous cells is realized with the aid of F_{671}. The released F_{508} in live cells could

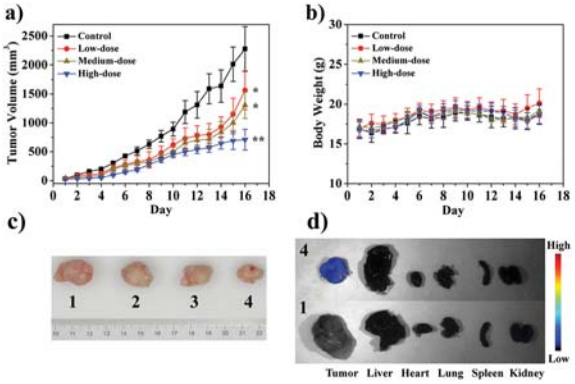

Fig. 5 Antitumor efficacy of F_{671}. (a) The HepG-2 tumor growth curves after different treatments. (b) The body weight variation of HepG-2 tumor-bearing mice during treatment. (c) Representative images of the HepG-2 tumors after dealing with different treatments on day 16 (1: control, 2: low-dose, 3: medium-dose, 4: high-dose). (d) Fluorescence images of the main internal organs after anatomy dissection (1: control group, 4: high-dose group). The error bars represent ±S.D. (n = 3). *P < 0.05, **P < 0.01.

act as a potent inhibitor to suppress the levels of HIF-1α, and facilitate the visualization of molecule release and distribution, as well as the verification of autophagic apoptosis induction. More importantly, F_{671} displays anticancer activity in various cancer cell lines and the HepG-2 tumor-bearing murine model. The specific cytotoxicity toward cancer cells and drug resistant cancer cells renders F_{671} a promising antitumor agent. To the best of our knowledge, this is the first time a dual-target BODIPY-based theranostic agent tested *in vitro* and *in vivo* has been reported.

This work is supported by the National Natural Science Foundation of China (21475059, 21527809 and 21775069).

Conflicts of interest

There are no conflicts to declare.

Notes and references

1 C. Holohan, S. Van Schaeybroeck, D. B. Longley and P. G. Johnston, *Nat. Rev. Cancer*, 2013, **13**, 714–726.
2 (*a*) R. W. Johnstone, A. A. Ruefli and S. W. Lowe, *Cell*, 2002, **108**, 153–164; (*b*) L. Kelland, *Nat. Rev. Cancer*, 2007, **7**, 573–584; (*c*) J. C. Yu, Y. Q. Zhang, X. L. Hu, G. Wright and Z. Gu, *Ann. Biomed. Eng.*, 2016, **44**, 1931–1945.
3 (*a*) A. S. Morgan, P. J. Ciaccio, K. D. Tew and L. M. Kauvar, *Cancer Chemother. Pharmacol.*, 1996, **37**, 363–370; (*b*) S. Aliya, P. Reddanna and K. Thyagaraju, *Mol. Cell. Biochem.*, 2003, **253**, 319–327.
4 (*a*) D. M. Townsend and K. D. Tew, *Oncogene*, 2003, **22**, 7369–7375; (*b*) E. Laborde, *Cell Death Differ.*, 2010, **17**, 1373–1380.
5 (*a*) T. G. Graeber, C. Osmanian, T. Jacks, D. E. Housman, C. J. Koch, S. W. Lowe and A. J. Giaccia, *Nature*, 1996, **379**, 88–91; (*b*) A. L. Harris, *Nat. Rev. Cancer*, 2002, **2**, 38–47.
6 (*a*) G. L. Semenza, *Trends Mol. Med.*, 2002, **8**, S62–S67; (*b*) G. L. Semenza, *Nat. Rev. Cancer*, 2003, **3**, 721–732.
7 (*a*) H. Zhong, A. M. De Marzo, E. Laughner, M. Lim, D. A. Hilton, D. Zagzag, P. Buechler, W. B. Isaacs, G. L. Semenza and J. W. Simons, *Cancer Res.*, 1999, **59**, 5830–5835; (*b*) G. L. Semenza, *Oncogene*, 2010, **29**, 625–634.
8 (*a*) A. Sau, F. P. Trengo, F. Valentino, G. Federici and A. M. Caccuri, *Arch. Biochem. Biophys.*, 2010, **500**, 116–122; (*b*) Y. Xia, H. K. Choi and K. Lee, *Eur. J. Med. Chem.*, 2012, **49**, 24–40; (*c*) S. Chen and N. Sang, *J. Cell. Biochem.*, 2016, **117**, 267–278.
9 (*a*) M. H. Lee, J. L. Sessler and J. S. Kim, *Acc. Chem. Res.*, 2015, **48**, 2935–2946; (*b*) R. Kumar, W. S. Shin, K. Sunwoo, W. Y. Kim, S. Koo, S. Bhuniya and J. S. Kim, *Chem. Soc. Rev.*, 2015, **44**, 6670–6683; (*c*) J. C. Yu, Y. L. Chen, Y. Q. Zhang, X. K. Yao, C. G. Qian, J. Huang, S. Zhu, X. Q. Jiang, Q. D. Shen and Z. Gu, *Chem. Commun.*, 2014, **50**, 4699–4702; (*d*) P. Parhi, C. Mohanty and S. K. Sahoo, *Drug Discovery Today*, 2012, **17**, 1044–1052.
10 (*a*) G. Ricci, F. De Maria, G. Antonini, P. Turella, A. Bullo, L. Stella, G. Filomeni, G. Federici and A. M. Caccuri, *J. Biol. Chem.*, 2005, **280**, 26397–26405; (*b*) L. Federici, C. Lo Sterzo, S. Pezzola, A. Di Matteo, F. Scaloni, G. Federici and A. M. Caccuri, *Cancer Res.*, 2009, **69**, 8025–8034.
11 A. Bessette and G. S. Hanan, *Chem. Soc. Rev.*, 2014, **43**, 3342–3405.
12 J. D. Hayes, J. U. Flanagan and I. R. Jowsey, *Annu. Rev. Pharmacol. Toxicol.*, 2005, **45**, 51–88.
13 (*a*) Y. H. Hung, L. M. Chen, J. Y. Yang and W. Y. Yang, *Nat. Commun.*, 2013, **4**, 2111–2117; (*b*) L. He, C. P. Tan, R. R. Ye, Y. Z. Zhao, Y. H. Liu, Q. Zhao, L. N. Ji and Z. W. Mao, *Angew. Chem., Int. Ed.*, 2014, **53**, 12137–12141 (*Angew. Chem.*, 2014, **126**, 12333–12337); (*c*) L. He, Y. Li, C. P. Tan, R. R. Ye, M. H. Chen, J. J. Cao, L. N. Ji and Z. W. Mao, *Chem. Sci.*, 2015, **6**, 5409–5418.
14 C. Maiuri, E. Zalckvar, A. Kimchi and G. Kroemer, *Nat. Rev. Mol. Cell Biol.*, 2007, **8**, 741–752.
15 N. Mizushima, T. Yoshimori and B. Levine, *Cell*, 2010, **140**, 313–326.
16 C. X. Chen, J. Cao, X. Y. Ma, X. B. Wang, Q. Y. Chen, S. H. Yan, N. W. Zhao, Z. R. Geng and Z. L. Wang, *Sci. Rep.*, 2016, **6**, 20853–20864.
17 Z. von Marschall, T. Cramer, M. Hocker, G. Finkenzeller, B. Wiedenmann and S. Rosewicz, *Gut*, 2001, **48**, 87–96.
18 R. D. Guzy, B. Hoyos, E. Robin, H. Chen and L. Liu, *Cell Metab.*, 2005, **1**, 401–408.
19 L. Helbig, L. Koi, K. Bruchner, K. Gurtner, H. Hess-Stumpp, K. Unterschemmann, M. Baumann, D. Zips and A. Yaromina, *Radiat. Oncol.*, 2014, **9**, 207–216.
20 (*a*) D. Hockenbery, G. Nunez, C. Milliman, R. D. Schreiber and S. J. Korsmeyer, *Nature*, 1990, **348**(6299), 334–336; (*b*) J. M. Adams and S. Cory, *Science*, 1998, **281**, 1322–1326.
21 (*a*) N. A. Thornberry and Y. Lazebnik, *Science*, 1998, **281**, 1312–1316; (*b*) A. G. Porter and R. U. Janicke, *Cell Death Differ.*, 1999, **6**, 99–104.